JOURNAL OF GUIDANCE, CONTROL, AND DYNAMICS
Vol. 20, No. 5, September–October 1997

Autonomous Optical Guidance and Navigation Strategy Around a Small Body

Jun'ichiro Kawaguchi,* Tatsuaki Hashimoto,† Takashi Kubota,‡ and Shujiro Sawai§
Institute for Space and Astronautical Science, Kanagawa 229, Japan
and
Gene Fujii¶
International Space University, Illkirch 67400, France

An impending demand for exploring small bodies such as comets and asteroids initiated the Japanese MUSES-C mission to the near-Earth asteroid Nereus, where it will touch down on the surface. Autonomous optical guidance and navigation strategies around the asteroid is discussed. An aligned intercept guidance that enables the approach from the prescribed direction is built, together with some important guidance properties associated with it. Among them, a combined range-estimation technique using corrections without a range sensor is derived. The robust feature of the closed-loop guidance scheme is stressed. For the first time concrete strategies for such missions to small bodies are presented. Some comprehensive numerical illustrations, including gravity effects, are given from the MUSES-C mission to support the discussion.

Nomenclature

$\boldsymbol{a}$	= acceleration vector
$\boldsymbol{b}$	= bias vector
$\boldsymbol{e}$	= line-of-sight unit vector
F, F^*	= Fourier spectra of the images
$\boldsymbol{f}$	= translation shift vectors
$f(\bullet)$	= image intensity distribution, amplification factor
$g, g(\bullet)$	= gravity, filter attenuation
H, H_0	= altitude, initial altitude
$\boldsymbol{h}$	= angular momentum vector
I	= illumination compensation
k	= damping factor
$\boldsymbol{p}$	= prescribed approach vector
r	= distance
r^*	= end distance of phase D-I
$\boldsymbol{r}$	= position vector
s	= Laplace operator
$\boldsymbol{s}$	= sun direction unit vector
T_s	= time for settlement
t	= time
t^*	= time to be guided
v	= descent velocity
v^*	= specified descent velocity
x, y	= coordinate variables
$\boldsymbol{z}$	= guidance variable vector
α	= attenuation factor
β, β'	= acceleration factors
$\Delta T_c, \Delta T_c\text{-}II$	= correction time intervals
ΔT_n	= navigation time interval
Δt	= time-to-go parameter
$\Delta \boldsymbol{V}$	= maneuver acceleration, velocity increment
$\Delta x, \Delta y$	= image shift amounts
$\Delta\theta$	= image-frame rotation angle
$\Delta\theta_0^*$	= camera angular resolutions
$\delta(\bullet)$	= variation operator
ε	= dispersion, or threshold
η, ξ	= Fourier spectrums
Θ	= body to inertial transform
κ	= nondimensional time-to-go
$\lambda_e, \lambda_{\dot{e}}, \lambda_h$	= acceleration components
$\lambda'_e, \lambda'_{\dot{e}}, \lambda'_h$	= correction components
μ	= bouncing coefficient
ρ	= range
σ	= standard deviation
τ, τ_f	= filter time constants
χ	= correction interval
ψ	= asteroid coordinate transform
ω	= rotation angular velocity

Superscripts and subscripts

att	= attitude
d	= descent
est	= estimate
obs	= observed
rel	= relative
rot	= rotation
s/c	= spacecraft
T	= transposed
t	= true
ω	= rotation angular rate
$\|\bullet\|$	= vector norm operator
$[\bullet]$	= vector operator
//	= parallel
$+, -$	= post and pre
$\hat{}$	= estimate, body-fixed expression

Received Dec. 29, 1996; revision received June 12, 1997; accepted for publication June 13, 1997.

*Associate Professor, Systems Engineering, 3-1-1 Yoshinodai, Sagamihara. E-mail: jkawa@newslan.isas.ac.up. Member AIAA.
†Associate Professor, Spacecraft Engineering, 3-1-1 Yoshinodai, Sagamihara.
‡Research Associate, Spacecraft Engineering, 3-1-1 Yoshinodai, Sagamihara.
§Research Associate, Systems Engineering, 3-1-1 Yoshinodai, Sagamihara.
¶Postgraduate Student, Department of Aerospace Engineering, Parc d'Innovation, Boulevard Gonthier d'Andernach.

Introduction

SMALL body exploration is one of the most sophisticated missions currently being investigated.[1,2] Among them, the Japanese MUSES-C[1] of the Institute for Space and Astronomical Science (ISAS) to the near-Earth asteroid Nereus is scheduled to be launched in 2002 and will touchdown upon the surface and return samples to Earth. In guiding and navigating the spacecraft around the asteroid, the optical sensors are inevitably utilized autonomously onboard, due to the long communication time between the spacecraft and the Earth. This paper addresses how the autonomous guidance and navigation strategy is built for such missions. For the first time, a concrete

strategy is given, implicitly assuming the MUSES-C spacecraft as an example.

In view of past research on this subject, special attention has been given to orbital motion and stability around irregularly shaped small bodies.[3,4] As missions to these objects have been proposed such as Europe's ROSETTA mission to a comet nucleus, an intensive planning strategy has been attempted,[5,6] which points out the necessity of autonomy in guidance and navigation. Recent investigations[7,8] also cover the autonomous optical navigation in these missions. Obviously, autonomy based on optical images requires image processing. The most conventional approach is to extract characteristic points and to assess their correlation,[9] which determines how much the image shifts and provides the translational motion by compensating for the attitude motion. In recent years, image processing has been associated more firmly with the navigation aspects, especially for small body missions.[10,11] Optical measurements have been applied mostly to orbit determination analyses[12–14]; however, almost all of the studies so far distinguish the navigation from the guidance and, typically, have reported how the orbit determination is carried out via the optical measurements. What is important is that not all of the orbital information is required for guidance to the small body. Both the navigation and the guidance have to be examined tactically in view of what is necessary and sufficient. For the most part, the orbital correction schemes used for guidance are classical because they rely on the conventional state vector estimates. Therefore, navigation strategies have recently been reexamined from the guidance aspects.[15–17] Here closed-loop orbit control onboard is stressed, whereas existing approaches are a type of open-loop control. A purely proportional guidance is the most straightforward closed-loop strategy so far employed, the extension of which is emphasized in this paper.

First discussed is the flight phase decomposition rationally in view of the sensor availability and guidance objectives. The image processing is presented second, through which the line-of-sight (LOS) rate information is retrieved by correlating the images taken onboard. This technique excludes fragile characteristic point tracking, making a fixed camera available. What is stressed is an extended intercept guidance strategy that guarantees the prescribed approach direction. The discussion on a new combined range-estimation technique along with the guidance maneuvers follows. Then, the stability and accuracy assessment that tune the parameters are discussed. A discussion on the correction interval is presented last, which compares the optimal spacing rule[18] with the constant interval strategy in terms of fuel consumption. With these six new major schemes, the paper gives a numerical demonstration, in which the results support the discussion developed.

Mission Phases

Depending on the availability of the optical sensors and their coverage, the descent maneuvers are divided into five subphases. The spacecraft is assumed to carry a visible imager, optical navigation camera (ONC), a laser altimeter, light radar (LIDAR), and a laser range finder (LRF). The ONC assumed here has the field of view (FOV) of 30 × 30 deg, and it is available from 2000 km to 1 m altitude above the surface. The coverage of the LIDAR here is assumed within 50 km to 50 m above the surface. LRFs are required to measure the altitude accurately below 100 m. The spacecraft is also supposed to carry the target plates that are the artificial land marks with which the spacecraft can make a rendezvous, canceling out the horizontal relative velocity. The target body size assumed is less than 1 km in diameter, as later numerical examples will indicate. Provided the target body is made of silicate as is Earth, the surface gravity is around 0.1 mg, while the maneuver acceleration is typically higher than 1 mg, which dominates even the surface gravity.

Three distinct parameters determine how the phases are divided. 1) Diversity of image size: the target body is first seen as a single point from a distance, but eventually the target body spreads over the FOV. 2) Guidance objective: inasmuch as synchronizing with the surface at a distance is accompanied by significant fuel consumption, it may as well be postponed as late and as close as possible. Therefore, the guidance at distant positions needs to be done with respect to the inertial frame. 3) Range information availability: beyond the distance of 50 km, the assumed LIDAR does not function and the guidance must be carried out based either on the a priori plan or on the range estimate built onboard. Both the LIDAR and LRF provide the range measurement only in the closest approach area. As a result, the phase is decomposed into five subphases listed in Table 1: rendezvous (R), descent-I (D-I), descent-II (D-II), decision and departure point (DDP), and touchdown (TD) phases. Note that the spacecraft will not orbit the asteroid, thus avoiding the orbital instability as a result of its irregular shape.

In phase R, the ground-based radio metric navigation accuracy is approximately from 300 to 1000 km at 1 AU from Earth. The flyby and rendezvous guidance is characterized by the ballistic parameter, which is defined as the distance from the target body to the incoming asymptote. While the relative velocity is maintained at a certain level with respect to the target body, the ballistic parameter is estimated relatively accurately via the so-called hybrid orbit determination method using both radiometric data and optical images.[12,14] Should the spacecraft stop with respect to the asteroid, the spacecraft heading would be unknown. Therefore, the spacecraft must continue approaching the body, maintaining an approach velocity of around 5–10 m/s, which is definitely larger than the radiometric navigation error. The flight period to the asteroid vicinity from 1000 km is only one day, and autonomous navigation is inevitably required.

To maintain solar power availability and the feature image visibility, it is preferable to approach from the prescribed direction, which is postulated here as 30 deg inclined in the afternoon side of the sun, that is, 14:00 in local solar time. Not only an intercept but an aligned approach are to be accomplished at the same time. An aligned intercept concept is introduced throughout all of the phases, which guides the trajectory compliant with the prescribed path using the LOS vector and its time derivative, both of which are easily calculated onboard.

Once the spacecraft is within the LIDAR coverage (50 km, where phase D-I starts), the combination of the ONC and the LIDAR constitutes the three-dimensional real-time navigator onboard. The descent velocity is reduced to 1 m/s. When the target image becomes larger and exceeds the FOV, the subcamera or sub-LIDAR point is unidentifiable without matching the images with the terrain map obtained beforehand. Because the ONC's FOV is approximately 30 deg here and the typical asteroid diameter is 500 m–1 km, the critical distance is approximately 2 km from the asteroid (phase D-II starts). There are two kinds of strategies in phase D-II. One is to leave the spacecraft coasting, and the other is to correct the path actively. If guided, the difficulty lies in the computer image processing. Usually, correlating the map and the images is a heavy burden not only in required computing speed but also in memory storage. The later

Table 1 Phase decomposition and definitions

	Phase R	Phase D-I	Phase D-II	Phase DDP	Phase TD
Range, km	2000–50	50–2	2–0.1	0.1	0.1–0
Descent speed, m/s	10–5	1	1–0.1	0.1	0.1
Optical sensors	ONC	ONC, LIDAR	ONC, LIDAR	ONC, LIDAR	ONC, LIDAR, LRF, target plate
Navigational information	LOS, LOS rate, range estimate	LOS, LOS rate, range	LOS, LOS rate, range	LOS, LOS rate, range	LOS, LOS rate, range
Guidance	Aligned intercept inertial descent	Aligned intercept inertial descent	Coasting inertial descent	Coasting transition	Aligned intercept synchronized
Target image	Entire	Entire	Partial	Partial	Partial

discussions conclude that a coasting strategy be implemented for D-II only with the descent velocity control of 1–0.1 m/s.

Phase DDP, one of the most important events, is where the touchdown point is specified and the final descent starts. Determining the touchdown point is too sophisticated for the spacecraft to carry out autonomously. This scenario assumes that the phase DDP decision can be handled on the ground during phase D-II. The autonomous touchdown point determination is left as a backup. This ground interface is not the primary item in this paper. The TD phase is the final approach period, in which the touchdown velocity vector is controlled to coincide with the local vertical direction on the surface with reduced descent speed of 0.1 m/s. It is difficult to obtain the horizontal velocity information, since the LRF measurement has little sensitivity to the oblique path and no Doppler sensors are assumed. In the MUSES-C, this difficulty is circumvented by placing an artificial landmark, a target plate, on the surface, which enables the spacecraft to rendezvous with it.[1] The local vertical information is obtained via LRF, while the nominal direction is uplinked from the ground prior to DDP. The place where the target plate settles is not controlled rigorously as specified. It is used for the cancellation of the horizontal relative motion with respect to the surface.

Throughout the phases, the use of LOS rate enables a fixed camera aperture direction to navigate the spacecraft without any gimbaling. With the camera direction frozen, the image is controlled to stay at the center of the FOV by guiding the spacecraft correctly using the LOS rate vector.

Image Processing and Illumination Compensation

The descent path penetrates the body if the LOS rate with respect to the body is controlled to zero. This is the fundamental principle of proportional guidance. Either the gimbaling a camera or tracking an object technique can be used to output the LOS rate at a distance, while the target is seen as a single point. However, the difficulty shows up in the case when the spacecraft approaches very close to the surface and the image spreads over the FOV. In such geometry, there is not an automatic tracking rationale specifying what object should be tracked. This paper proposes a different strategy that never tracks any object at all. Even with the fixed-orientation camera onboard, the LOS rate information can be obtained from two images. It is accomplished by shifting the images in reference to each other so that the correlation is maximized, which gives the displacement in the known time interval. Note that this process does not require knowledge of the LOS direction itself. The primary advantage of this is its high robustness for any terrain feature because the whole image information is utilized. And the trajectory control loop can be freed from the complicated camera tracking scheme. Contemporary image processing utilizes two kinds of hardware. One is the so-called optical flow processor that detects the pixel shift very efficiently. The other is the fast Fourier transformation (FFT) processor that is commonly used. Provided the two-dimensional image signal is obtained as $f(x, y)$, the Fourier spectra are obtained as

$$F(\xi, \eta) = \iint f(x, y) e^{-jx\xi} e^{-jy\eta}\, \mathrm{d}x\, \mathrm{d}y \tag{1}$$

If the next image is shifted $x + \Delta x$, $y + \Delta y$ with the FOV rotation angle of $\Delta\theta$, the corresponding spectra F^* should take the form

$$F^*(\xi, \eta) = \exp[-j(\Delta x\xi + \Delta y\eta)] F(\xi \cos\Delta\theta + \eta \sin\Delta\theta, -\xi \sin\Delta\theta + \eta \cos\Delta\theta) \tag{2}$$

The results indicate that the spectra are also rotated in the frequency domain, while the translational displacements affect only the spectra phase. When the spectra are examined in terms of the phase at several distinct frequencies, the translational motion is estimated uniquely by neglecting $\Delta\theta$. The spectral intensity distribution again gives the rotation information, if the spectra F and F^* are processed with respect to $\Delta\theta$ via another FFT. Thus, the bootstrap process works theoretically, and the two kinds of motion, translational and rotational shifts, are estimated from two images. Note that the entire image information is utilized to make this estimate. In actual applications, double-FFT sometimes does not function as anticipated because the images usually do not contain enough frequency information. One breakthrough is to use the calculated spacecraft attitude motion available onboard, which provides the translational shifts directly. Another way is to divide the image plane into several subimages. Provided the translational displacements $\boldsymbol{f}_i^k$ are calculated for the ith subimage on the kth frame via FFT, both the rotational and translational displacement vectors ε and $\boldsymbol{b}$ are obtained through the least square method, for instance, minimizing

$$\sum \left\{ \boldsymbol{f}_i^{k+1} - \varepsilon \times \boldsymbol{f}_i^k - \boldsymbol{b} \right\}^2$$

The illumination conditions strongly affect the LOS direction accuracy, except while the spacecraft is at a distance. An intercept itself does not require the LOS direction; however, the landing area may as well be targeted and the difference between the center of illumination and the center of the body directions must be compensated. The spacecraft needs to be equipped with the illumination corrector δI onboard, which outputs the LOS correction $\delta \boldsymbol{e} = \delta I(\boldsymbol{e}, \rho, t)$. A certain iteration may be required to account for the measured illumination center.

Aligned Intercept Guidance

Basic Guidance Relations

A great deal of research has been reported concerning the proportional guidance scheme, especially in missile technology.[16] The fundamental idea is that the LOS vector is frozen inertially so that the spacecraft can hit the target. Provided the target body is in an acceleration-freefield, the relative motion $\boldsymbol{r}$ of the spacecraft around the asteroid is described by

$$\ddot{\boldsymbol{r}} = \ddot{\boldsymbol{r}}_{\text{target}} - \ddot{\boldsymbol{r}}_{\text{s/c}} = \boldsymbol{a}, \qquad \ddot{\boldsymbol{r}}_{\text{s/c}} = -\boldsymbol{a} \tag{3}$$

Here, a throttleable propulsion system is assumed for the discussion, in which the thrust acceleration $\boldsymbol{a}$ is expressed by the linear combination of the LOS vector $\boldsymbol{e}$, its derivative $\dot{\boldsymbol{e}}$, and the angular momentum vector $\boldsymbol{h}$ components: $\boldsymbol{a} = -(\lambda_e \boldsymbol{e} + \lambda_{\dot{e}} \dot{\boldsymbol{e}} + \lambda_h \boldsymbol{h})$. Inasmuch as the angular momentum quantity is expressed as $\boldsymbol{h} = \boldsymbol{r} \times \dot{\boldsymbol{r}}$, the magnitude of $\boldsymbol{h}$ behaves according to

$$\dot{h} = -(\lambda_{\dot{e}}/r) h \tag{4}$$

This relation suggests that the angular momentum magnitude is frozen if the LOS rate component is zero even under the maneuvers. And the appropriate choice of the thrust direction guarantees the continuous decrease of the angular momentum. Thus, this scheme is called proportional guidance, because the thrust only has to be generated just proportional to the LOS rate direction. The simple expression, $h = r^2 \|\dot{\boldsymbol{e}}\|$ indicates that such a maneuver makes the LOS rate zero. Note that the angular momentum control is equivalent to proportional guidance.

Through manipulation, the following time history of $\|\dot{\boldsymbol{e}}\|$ is derived:

$$\frac{\mathrm{d}\|\dot{\boldsymbol{e}}\|}{\mathrm{d}t} = \frac{-(\lambda_{\dot{e}} + 2\dot{r})\|\dot{\boldsymbol{e}}\|}{r} \tag{5}$$

If $|\lambda_{\dot{e}}| \gg |\dot{r}|$ is satisfied, the distance information is directly derived through the combination of LOS rate magnitude, its time derivative, and the maneuver component. Note that the distance information cannot be extracted without active control ($\lambda_{\dot{e}} = 0$) because the LOS rate history never determines the path uniquely. Later the impulsive maneuver discussion presents a more practical range estimation scheme that can work along with the guidance maneuver.

Aligned Intercept Guidance[16]

It is assumed that the spacecraft is supposed to approach from the prescribed direction. As the guidance metric, the angle between the LOS and the prescribed descent direction is taken as the guidance variable $\boldsymbol{z} = \boldsymbol{e} \times \boldsymbol{p}$ where $\boldsymbol{p}$ is the prescribed approach direction. Provided the trajectory maneuver is applied at t_k, represented by the velocity increment $\Delta \boldsymbol{V}_k$, if the property $r\boldsymbol{z}$ is required to vanish at t^*, then

$$\boldsymbol{0} = (\dot{\boldsymbol{r}}_k + \Delta \boldsymbol{V}_k) \times \boldsymbol{p} \cdot \Delta t + (\boldsymbol{r}_k \times \boldsymbol{p}) \tag{6}$$

where Δt is the time interval from t_k to t^*. It is assumed that $\Delta \boldsymbol{V}_k$ should be perpendicular to the sun direction $\boldsymbol{s}$, taking the spacecraft configuration into account. Without loss of generality, the spacecraft is assumed to orient the solar cell panel to the sun direction, whose thrusters are perpendicular to it. The solution to this is obtained by taking the cross product of $\boldsymbol{s}$ and Eq. (6), which gives the impulsive guidance strategy making z_k zero:

$$\Delta \boldsymbol{V}_k = -\frac{r_k}{(\boldsymbol{s}^T \boldsymbol{p})}\left\{\left[\boldsymbol{s} \times \left(\dot{\boldsymbol{z}}_k + \frac{\dot{r}_k}{r_k}\boldsymbol{z}_k\right)\right] + \frac{1}{\Delta t}(\boldsymbol{s} \times \boldsymbol{z}_k)\right\} \tag{7}$$

When Δt gets shorter, the guidance is degenerated just to the feedback of the guidance parameter without any damping. On the other hand, if Δt becomes longer, the guidance is dominated by damping. Similarly, the requirement of the angular momentum to vanish instantaneously and the attitude constraint give the following angular momentum control through the similar manipulation:

$$\Delta \boldsymbol{V}_k = -\frac{r_k}{(\boldsymbol{s}^T \boldsymbol{e}_k)}[\boldsymbol{s} \times (\dot{\boldsymbol{e}}_k \times \boldsymbol{e}_k)] \tag{8}$$

In a particular case when $\boldsymbol{s}$ is equal to $\boldsymbol{e}$, the angular momentum control $\Delta \boldsymbol{V}_k = -r_k \dot{\boldsymbol{e}}_k$ is derived, which is the proportional guidance. The following two propositions support the guidance scheme developed.

Proposition 1: If $\dot{\boldsymbol{e}} = \boldsymbol{0}$, then $\dot{\boldsymbol{z}} = \boldsymbol{0}$. This is obviously true and an intercept always implies that the guidance variable $\boldsymbol{z}$ is constant.

Proposition 2: If $\boldsymbol{z} = \boldsymbol{0}$, then $\dot{\boldsymbol{e}} = \boldsymbol{0}$.

Proof: Here $\boldsymbol{z} = \boldsymbol{0}$ indicates $\boldsymbol{e} \,//\, \boldsymbol{p}$. Because $\boldsymbol{z}$ is constant implies either $\dot{\boldsymbol{e}} \,//\, \boldsymbol{p}$ or $\|\dot{\boldsymbol{e}}\| = \boldsymbol{0}$. If both $\dot{\boldsymbol{e}} \,//\, \boldsymbol{p}$ and $\boldsymbol{e} \,//\, \boldsymbol{p}$ hold true at the same time, it is contradictory. Therefore, $\|\dot{\boldsymbol{e}}\| = \boldsymbol{0}$. QED

These propositions insist that whenever the guidance variable $\boldsymbol{z}$ is made zero, the intercept is always accomplished. In other words, an aligned intercept concept is an extended scheme that guarantees the intercept.

Combined Range Estimation Along with Guidance Maneuvers

At a great distance, range measurement is not available and obtaining the range estimate is highly advantageous in terms of securing the approach, even though the accuracy is very degraded. As for the continuous acceleration maneuvers, Eq. (5) is manipulated for the range estimate as follows:

$$\hat{\boldsymbol{r}}_{\text{range}} \cong -\lambda_{\dot{e}} \Big/ \frac{\mathrm{d}}{\mathrm{d}t}\{\ell_n \|\dot{\boldsymbol{e}}\|\} \tag{9}$$

In case of impulsive maneuvers, the angular momentum is discretely changed at the instant of the maneuver. Decomposing as $\Delta \boldsymbol{V}_k = -(\lambda'_e \boldsymbol{e}_k + \lambda'_{\dot{e}} \dot{\boldsymbol{e}}_k + \lambda'_h \boldsymbol{h}_k)$, the range estimate is obtained by the following equation:

$$\hat{r}_k = |\lambda'_{\dot{e}}| \cdot \|\dot{\boldsymbol{e}}_k^-\|^2 \cdot \left|\left(\dot{\boldsymbol{e}}_k^{+T} \dot{\boldsymbol{e}}_k^-\right) - \left\|\dot{\boldsymbol{e}}_k^-\right\|^2\right|^{-1}$$

$$\left(\cong |\lambda'_{\dot{e}}| \cdot \|\dot{\boldsymbol{e}}_k\| \cdot \left|\left\|\dot{\boldsymbol{e}}_k^+\right\| - \left\|\dot{\boldsymbol{e}}_k^-\right\|\right|^{-1}\right) \tag{10}$$

The simple structure of this estimation scheme should be emphasized. It is composed only of $\dot{\boldsymbol{e}}$ and $\lambda'_{\dot{e}}$. Equation (10) is also derived from an extreme case of Eq. (9). The estimation never requires navigation-specific maneuvers for this purpose and can be carried out along with the guidance maneuvers. It should be pointed out that the range estimate may become indefinite for very small maneuvers. This difficulty is circumvented by excluding the erroneous estimates and introducing a certain low-pass filter stabilizing the estimate. It is quite important to note that range information cannot be extracted if no maneuver is applied to the spacecraft.

Guidance Stability with Navigation Filters

Aligned Intercept Guidance Stability and LOS Rate Filter

If the acceleration magnitude is normalized by β', the guidance law for a spacecraft propelled by continuous propulsion is expressed from Eq. (7) as

$$\boldsymbol{a} = -\beta'\{(\boldsymbol{s} \times \boldsymbol{z}_k) + k(\boldsymbol{s} \times \dot{\boldsymbol{z}}_k)\} \tag{11}$$

When the equation of motion $\ddot{\boldsymbol{r}} = r\ddot{\boldsymbol{e}} + 2\dot{r}\dot{\boldsymbol{e}} + \ddot{r}\boldsymbol{e}$ is multiplied by $\boldsymbol{p}$, rewriting $\beta'(\boldsymbol{s}^T \boldsymbol{p}) = \beta$, the characteristic equation representing guidance stability is derived:

$$r\ddot{\boldsymbol{z}} + (2\dot{r} + k\beta)\dot{\boldsymbol{z}} + (\ddot{r} + \beta)\boldsymbol{z} = \boldsymbol{0} \tag{12}$$

The magnitude of $\boldsymbol{z}$ is decreasing if $(2\dot{r} + k\beta) > 0$ and $(\ddot{r} + \beta) > 0$. Because $\boldsymbol{z}$ magnitude becomes zero implies that the approach direction coincides with the prescribed path vector $\boldsymbol{p}$. The angular momentum becomes zero at the same time, because $\boldsymbol{z}$ becomes constant. It should be pointed out that the conventional angular momentum control law guarantees only that $\boldsymbol{z}$ becomes constant.

In most cases, LOS rate signal is highly contaminated with noise and a certain filter needs to be introduced, such as $\dot{z}_k(s) = 1/(1 + \tau s) \cdot \dot{z}_{k,\text{true}}(s)$. Assuming $\|\ddot{r}\| \ll \beta$, the following characteristic equation is obtained, similar to Eq. (12):

$$r\tau s^3 + (r + 2\dot{r}\tau)s^2 + (\beta k)s + \beta \cong 0 \tag{13}$$

The necessary conditions for stability are derived as follows:

$$r > -2\dot{r}\tau, \qquad [1 + (2\dot{r}\tau)/r]k > \tau \tag{14}$$

The first requirement states that the guidance is stable beyond the stability boundary distance that is determined by the product of the approach velocity and the filter time constant. The second condition is simplified in a distant location as $k > \tau$, which requires that the artificial damping should prevail over the filter time delay. In regard to the artificial damping coefficient k, it is frequently represented by the so-called time-to-go parameter Δt onboard such as $k = (-r/\dot{r}) \cdot \kappa = \Delta t \cdot \kappa$. To secure satisfactory damping, the stability requirement on the filter time constant is rewritten as $\Delta t = (-r/\dot{r}) > (1/\kappa + 2)\tau$.

Descent Rate Control and Altitude Filters

An important parameter of concern is the descent rate. The following descent rate guidance logic performed every ΔT_c correction interval is employed:

$$\dot{H}_{k+1} = \dot{H}_k - k\left(\frac{H_k - H_{k-1}}{\Delta T_c} - v^*\right) \tag{15}$$

Stability inspection indicates that $0 < k < 1$ will be assured. In practical applications, the altitude is $H_k = r_k - R$ and the rotational motion of the asteroid may affect the altitude control causing some residual error, because the terrain height fluctuates and $\dot{R} \neq 0$. A certain navigation filter must be introduced especially during phase TD that requires a very slow descent rate of around 0.1 m/s. Suppose the altitude filter of $\hat{H}_k(s) = 1/(1 + \tau s) \cdot H_{k,\text{true}}(s)$ is incorporated; through the mathematical stability analysis, the aforementioned necessary condition is altered to $0 < k < (1 + \tau/\Delta T_c)^{-1}$.

The gravity field around small bodies is very faint. However, if made of silicate, the 0.64-km-radius asteroid surface gravity is approximately 0.1 mg, which accelerates the spacecraft up to 1 m/s during hovering for 1000 s. This threatens to substantially disturb the descent rate control. The most straightforward breakthrough is to add the feedforward term in the scheme as

$$\dot{H}_{k+1} = \dot{H}_k - k\left(\frac{H_k - H_{k-1}}{\Delta T_c} - v^*\right) + v_{\text{forward}} \tag{16}$$

In principle, the gravity compensation amount is given as $v_{\text{forward}} = \Delta T_c \cdot \hat{\mu}/(\hat{R} + r_{\text{range}})^2$. The gravity constant and the radius knowledge are not precisely available and such errors in the parameters contribute to the descent rate residuals.

Optimal Spacing and Correction Interval

In most interplanetary flights, trajectory correction takes place at times determined by how much fuel is needed to achieve the admissible terminal dispersion. The allocation of the correction interval is the so-called spacing problem, which has been intensively studied for many years. The same concept is applied for this approach guidance. Provided that the velocity and position navigation errors are represented by λ and ρ, the optimal spacing rule states that the

flight period left to the terminal point T_k at kth correction point shall satisfy the relation[18]

$$T_k/T_{k+1} = T_{k-1}/T_k + (1/T_k)\cdot(2\rho/\lambda) \tag{17}$$

In optical navigation, both errors are approximately represented by $\lambda \approx r\|\dot{\boldsymbol{e}}\|/\Delta T_n$ and $\rho \approx r\|\dot{\boldsymbol{e}}\|$. And without loss of generality, $\Delta T_n \ll T_k$ is assumed to hold. Therefore, Eq. (17) is simplified to $T_k/T_{k+1} = T_{k-1}/T_k$, a constant ratio spacing. Spacing ratio is determined by the terminal error specification. It is important that the constant correction interval is not an optimal choice and the spacing rule may reduce the correction amount, depending on the navigation accuracy. The spacing ratio of 1 is obviously one solution, which corresponds to the continuous correction scheme. The later numerical example shows the advantage of this spacing rule.

Phase-Specific Guidance Strategies

Phases R and D-I

During these segments, the target is seen as a small dot and the spacecraft vector to the target body is well defined from the images through the illumination compensation. The guidance strategy of

$$\Delta \boldsymbol{V}_k = -\frac{r_k}{(\boldsymbol{s}^T\boldsymbol{p})}\boldsymbol{s}\times\left\{\left[(\dot{\boldsymbol{e}}\times\boldsymbol{p}) - \frac{|v_{\rm rel}|}{r_k}(\boldsymbol{e}\times\boldsymbol{p})\right] + \frac{1}{\Delta t}(\boldsymbol{e}\times\boldsymbol{p})\right\} - k(v - v_{\rm rel})\boldsymbol{p} \tag{18}$$

gives the aligned intercept approach with the descent velocity control capability. In the phase R, the range measurement is not available and either programmed range or range estimate is substituted. Δt indicates the time-to-go parameter that is also built in onboard. LOS rate information is obtained via a low-pass filter. The mentioned spacing rule may be applied to phase R to reduce the correction velocity amount.

One of the most important events in the descent occurs when phase D-I ends. The touchdown point dispersion is governed then. In Fig. 1, the mechanism related to the miss-distance degradation is shown. Assuming the camera angular resolution is $\Delta\theta = g(\bullet)$ and the critical distance where the D-I ends is r^*, the final landing point dispersion ε is characterized by

$$\varepsilon = \{(r^* + v^*\Delta T_c)\Delta\theta + r^*\Delta\theta\}\frac{r^*}{\Delta T_c v^*}$$

And the following equations are obtained:

$$\varepsilon = r^* f(\chi) g(\alpha), \qquad f(\chi) = (2+\chi)/\chi$$
$$g\left(\alpha, \Delta\theta_0^*\right) = \Delta\theta_0^*\sqrt{(1-\alpha)/(1+\alpha)} \tag{19}$$

where χ is the nondimensional correction interval, $\chi = (v^*\Delta T_c)/r^*$, and α the filter attenuation factor, $\alpha = \exp(-\Delta T_n/\tau_f)$. $\Delta\theta_0^*$ is the standard deviation of the LOS angle measurement noise and $f(\bullet)$ is an important amplification factor whose typical figures are $f(0.25) = 9, f(0.5) = 5, f(1) = 3, f(2) = 2, f(10) = 1.2$, which implies that χ should be larger so that this amplification can be suppressed. How the landing dispersion is determined depends on the key parameters χ and α.

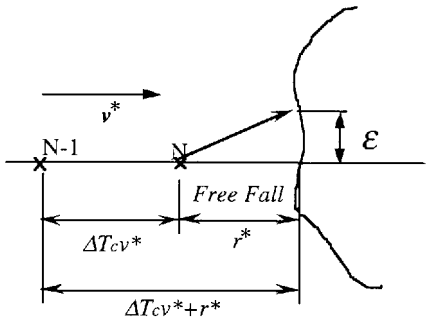

Fig. 1 Guidance miss-distance analysis.

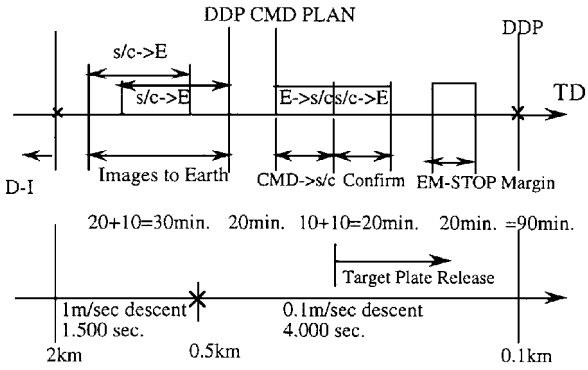

Fig. 2 Ground support at DDP.

Phase DDP

Phase D-II may as well be left coasting without any guidance corrections, before the guidance is switched over to the final descent and touchdown maneuvers. Figure 2 presents what kind of ground-based operations are typically required to initiate phase DDP. Where to land is probably the hardest thing for the spacecraft to determine autonomously. Fortunately, slowing down the descent velocity lengthens the phase D-II flight period to $1\frac{1}{2}$ h, which is enough time for communicating with the ground stations. At the ground stations, several images are accurately analyzed to give the ballistic parameter information together with the virtual closest approach time, both of which define the spacecraft path. The scenario in Fig. 2 consists of the command to the spacecraft, confirmation of the commands, and any required emergency operations.

Where to touchdown is decided at the altitude of 100 m above the surface, taking the LRF coverage into account. The subspacecraft point is defined as the touchdown point at DDP, whose local vertical direction coincides with the vector from the DDP to the subspacecraft point. It is assumed here that a detailed mapping period of a few months precedes the descent maneuvers discussed. Through the mapping phase, not only the topological information, but also the rotational state, is identified and accumulated on the ground. The local vertical direction is not only what the spacecraft descends along but is also the attitude that should be maintained all of the way. The landing attitude should be identical to the local vertical direction, which is input to the spacecraft at the DDP and corrected based on the LRF measurements. The direction is not constant but shifts along with the rotation motion of the asteroid. Such coordinate transformation is handled easily, even onboard, by referring to the ephemeris data. The greatest advantage of this plan is that the camera orientation is kept frozen.

Phase TD

An aligned intercept scheme using LOS rate information is also used, and it enables the touchdown direction to be locally vertical. The local terrain feature is compensated by LRF, which directly provides the local vertical direction in real time. As established in the descent rate control, this phase must employ the feedforward gravity compensation. The orbital motion transition takes place at the beginning of this phase: from the inertial approach to the descent synchronized with the surface motion. However, the closed-loop guidance scheme here does not require any extra transition information to make the motion synchronized. This is one of the most advantageous points in using this technique.

Practically speaking, the spacecraft MUSES-C is supposed to release a target plate as an artificial landmark with which the spacecraft rendezvous. No Doppler sensor is assumed for the MUSES-C. The target plate is introduced to allow sensing the horizontal velocity, which is not readily available onboard via the optical sensors. To this end, the target plate can be a small single light easily detected. Even if the target plate is not detected from the spacecraft, the image processing scheme introduced before makes use of the whole image information to extract LOS rate and the scheme functions without

Table 2 Phase R simulation statistical results

Case	Mean ΔV, m/s	$\Delta V(1\sigma)$, m/s	Mean align, deg	Align (1σ), deg	Mean B-p, km	B-p (1σ), km	Parameters
1	24.20	1.15	4.10	9.61	4.68	3.63	Nominal
2	19.84	0.58	1.23	0.91	3.45	2.52	$\Delta l = 150$ km
3	17.34	3.81	28.70	25.73	24.41	19.63	$\tau_f = 20{,}000$ s
4	38.78	0.59	0.83	0.42	3.37	1.53	$\Delta T_c = 150$ min, ΔT_c-$II = 30$ min

any reconfiguration. The release of the plate must precede the DDP, so that the spacecraft can acquire it after it settles onto the target's surface. Settling period is estimated by

$$T_s = \frac{H_0}{v_d} + 2\frac{\mu v_d}{g} + 2\frac{\mu^2 v_d}{g} + \cdots = \frac{H_0}{v_d} + \frac{2v_d}{g}\frac{\mu}{1-\mu} \qquad (20)$$

where H_0 is the release point altitude and v_d the plate descent velocity. Gravity here is approximately 0.1 mg, and the reflection coefficient μ is assumed about 0.1. Here μ indicates the reflected momentum with respect to that prior to the bouncing. One typical scenario may stipulate that the plate is released at the altitude of 265 m ($= H_0$) above the surface with 0.5 m/s ($= v_d$), while the spacecraft continues to descend at 0.1 m/s, so that the plate stops bouncing before the spacecraft reaches the DDP located at the altitude of 100 m.

Numerical Demonstration

The target body is numerically modeled as an ellipsoid whose three principal axes lengths are 250, 500, and 375 m. The rotation period is postulated as 5 h, with the spin axis normal to the ecliptic plane. The spacecraft is supposed to approach along the path on the ecliptic plane 30 deg inclined to the sun direction in the afternoon side, at the 14:00 o'clock time position.

The top of Fig. 3 shows the illumination compensation angle data during phase D-I in which the spacecraft approaches along path 30 and 35 deg inclined to the sun direction. Here, the approach speed is 1 m/s. The easiest way for the compensation may be to use the frozen offset parameters throughout the approach. As the following guidance examples indicate, the angular resolution of 10 arc min is baselined so that the touchdown point dispersion can be suppressed. Beyond the distance of 10 km, this offset parameter strategy works; however, this is no longer valid within 10 km and active illumination inversion software must be built onboard. The bottom of Fig. 3 examines the consequence of rotation period error on the illumination compensation. As easily recognized, if the rotation period is incorrectly modeled by 10%, the illumination compensation easily fails. This strongly suggests that the period must be identified accurately.

The guidance demonstrations to follow start from phase R, in which the initial distance is taken as 2000 km from the asteroid with the approach velocity v of 10 m/s. The descent path is defined 30 deg inclined to the sun direction on the ecliptic plane. The nominal navigation filter time constant τ_f of 2500 s is used, while the maneuver interval is 5 h (ΔT_c in Table 2). In this typical illustration, the initial lateral position error Δl of 300 km is postulated. The corresponding stability boundary distance defined by Eq. (14) is 100 km, which does not satisfy the stability requirement until the distance of 50 km. Therefore, on the way to the phase D-I transition point, the descent speed is decelerated to 5 m/s with the reduced filter time constant of 600 s and the correction interval of 60 min (ΔT_c-II in Table 2) to guarantee stability while maintaining the guidance accuracy. The simulation results are shown in Figs. 4 and 5. Figure 4 presents the trajectory-related properties associated with the proposed schemes. The aligned intercept guidance is required to assure the specified approach, and the results comply well. Figure 5 shows that the use of Eq. (10) with a low-pass filter gives the range estimate to a certain accuracy, especially within 500 km, even while the range is beyond the LIDAR coverage. The accuracy is approximately 10–30%, and this information can be regarded as the spacecraft location reference. LOS rate raw signal and filtered measurements are drawn on the same figure. The LOS rate signal fluctuates after 3000 min, which is caused by the updated navigation filter time constant of 600 s. The time when the range estimate

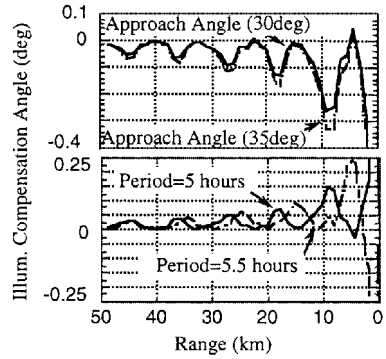

Fig. 3 Illumination compensation.

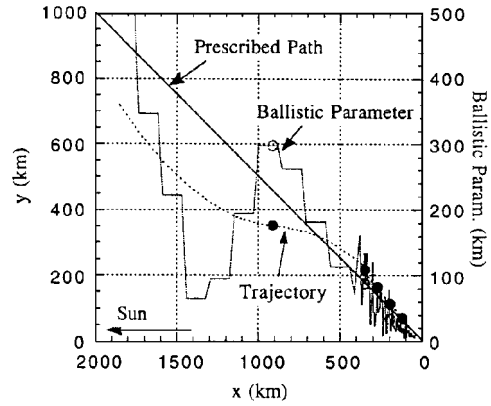

Fig. 4 Phase R: ballistic parameter and trajectory.

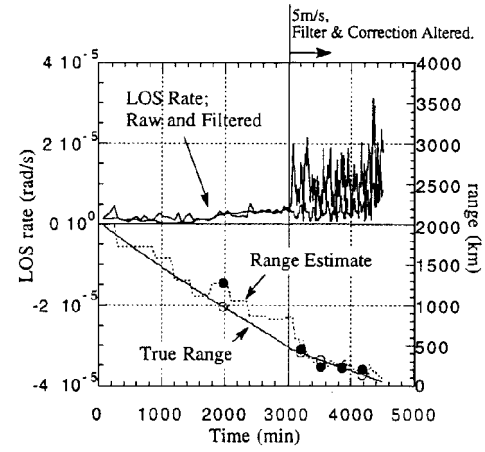

Fig. 5 Phase R: range estimate and LOS rate.

is available depends on the intensity of the LOS rate signal. The phase R ends when the spacecraft receives the LIDAR range alarm signal that the spacecraft is located within 50 km. When the phase R transitions to phase D-I, the ballistic parameter error is decreased to around 5 km. A statistical study was carried out, and the results are summarized subsequently. The results were obtained in a Monte Carlo manner, averaging 20 cases with the LOS measurement fluctuation equivalent to the resolution. Align and B-p in Tables 2–5 indicate the alignment angle ($\sin^{-1}|z|$) and the ballistic parameter distance, respectively.

It is concluded that the ΔV required from the distance of 2000 km is 24.2 m/s with standard deviation of 1.15 m/s. This figure includes the deceleration ΔV of 5 m/s on the way. Note that for the purpose

Table 3 Optimal spacing rule and constant correction interval strategy

Case	Mean ΔV, m/s	$\Delta V(1\sigma)$, m/s	Mean align, deg	Align (1σ), deg	Mean B-p, km	B-p (1σ), km	Spacing parameters
1	21.16	0.63	13.89	10.41	10.98	4.74	Spacing (ratio = 1.056, $\Delta V_{\text{lim}} = 0.5$ m/s)
1′	24.20	1.15	4.10	9.61	4.68	3.63	Constant (nominal, $\Delta V_{\text{lim}} = 0.5$ m/s)
2	32.56	0.64	1.73	0.90	4.93	3.23	Spacing (ratio = 1.056, $\Delta V_{\text{lim}} = 1.0$ m/s)
2′	37.86	1.25	1.85	1.03	4.69	2.99	Constant (nominal, $\Delta V_{\text{lim}} = 1.0$ m/s)
3	57.73	1.58	2.34	1.14	10.66	6.40	Spacing (ratio = 1.056, $\Delta V_{\text{lim}} = 2.0$ m/s)
3′	67.60	2.43	2.03	1.06	8.56	5.03	Constant (nominal, $\Delta V_{\text{lim}} = 2.0$ m/s)

Table 4 Phase D-I simulation statistical results

Case	Mean ΔV, m/s	$\Delta V(1\sigma)$, m/s	Mean align, deg	Align (1σ), deg	Mean B-p, m	B-p (1σ) m	Parameters
1	2.42	0.12	0.37	0.18	23.3	12.0	Nominal
2	2.65	0.11	0.58	0.22	39.2	17.4	$\tau_f = 2000$ s
3	1.77	0.04	0.44	0.25	37.1	19.5	$\Delta T_c = 60$ min
4	2.90	0.11	0.36	0.19	22.6	10.8	$\Delta l = 10$ km
5	2.71	0.09	3.87	0.22	128.8	10.8	$v = 2$ m/s

Table 5 Phase TD simulation statistical results

Case	Mean ΔV, m/s	$\Delta V(1\sigma)$, m/s	Mean align, deg	Align (1σ), deg	Mean B-p	B-p (1σ)	Parameters
1	0.34	0.04	4.82	2.32	13.2 cm	7.1 cm	Nominal
2	0.34	0.06	6.01	2.87	22.4 cm	11.1 cm	$\tau_f = 100$ s
3	0.21	0.02	6.44	2.71	33.8 cm	17.1 cm	$\Delta T_c = 120$ s
4	0.58	0.07	3.79	1.89	14.8 cm	7.1 cm	$\Delta l = 200$ m
5	0.32	0.03	73.44	6.21	51.1 m	52.9 m	$v = 20$ cm/s
6	6.61	0.01	6.74	3.69	22.1 cm	11.8 cm	$v = 10$ cm/s with gravity
7	4.98	0.15	15.05	7.43	1.9 m	1.0 m	$v = 10$ cm/s with C_{20}, C_{22}
8	4.88	0.31	18.96	12.07	1.5 m	0.9 m	Case 7 + spin period +10%
9	4.87	0.10	13.19	7.54	2.0 m	0.8 m	Case 7 + spin axis 0.1 rad
10	5.74	0.07	11.10	5.14	2.0 m	0.8 m	Case 7 + $\mu \times 1.2$
11	5.12	0.30	25.11	16.39	1.8 m	0.9 m	Case 7 + ΔV execution error 5%

of avoiding the extra fuel consumption, it is assumed here that the admissible largest limit for each correction is 0.5 m/s. The initial lateral position error contributes to the correction velocity amount; however, the sensitivity is not found to be high. In case 3, the stability boundary distance is 400 km, and the ballistic parameter is not controlled well, which proves the guidance stability dependence on the navigation filter time constant. As case 4 indicates, the shorter the correction interval becomes, the more accurate the guidance results get. In contrast to that, the correction velocity needs to increase. A certain practical compromised optimization is needed to tune the parameters.

As discussed in the preceding section, the optimal correction interval is never constant. An optimal spacing rule governs, which reduces the correction amount. Under the similar correction constraint, the spacing ratio of 1.056 in Eq. (17) is introduced, and the ΔV amount and the resulting guidance performances are assessed in Table 3. When the correction is limited to 0.5 m/s, while the total ΔV is reduced 3 m/s, the guidance performance is not degraded much. On the other hand, with the correction limited to 1 and 2 m/s, almost equivalent guidance performance is obtained with less total ΔV. Note that, in other words, the optimal spacing provides better guidance with the same ΔV budget. This does show the spacing rule advantage.

Phase D-I starts from a distance of 50 km, the LIDAR range. In view of the phase R results, the lateral position error of 5 km is typically considered in the simulations. The descent velocity is postulated as 1 m/s, which is tuned to satisfy the stability condition with the nominal navigation filter time constant of 600 s. The corresponding stability boundary is 1.2 km, which is within the end distance of phase D-I. The postulated correction interval is every 30 min. The spacing rule does not have to be adopted for this short period. Both the ballistic parameter and the guidance variable are well controlled to decrease asymptotically (top of Fig. 6) because the LOS rate signal is strong enough. The bottom of Fig. 6 shows the trajectory, which traces the prescribed approach line 30 deg inclined to the sun direction. The required ΔV from 50 km is estimated as

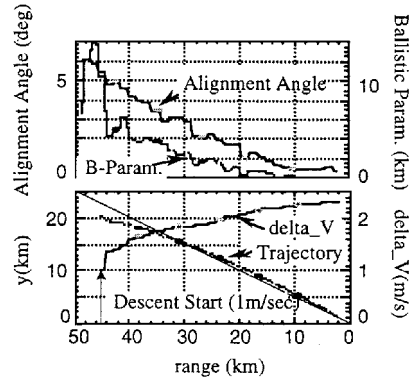

Fig. 6 Phase D-I: guidance results.

2.3 m/s including the departure velocity increment of 1 m/s. Monte Carlo-like statistics of 100 cases (Table 4) show that the ΔV of 2.42 m/s is required in phase D-I. As is easily noted, the instability occurs in case 5; this phenomenon was previously discussed. As case 4 suggests, the proposed guidance scheme is still robust for the large initial position error. Lengthening the correction time interval reduces the terminal dispersion errors with the benefit of less correction ΔV. It is concluded that the landing point dispersion is about 20–40 m on average.

Phase D-II is assumed as the coasting period. In this numerical example, the TD phase is examined from the altitude of 100 m. The trajectory plot in phase TD is shown in the top of Fig. 7, which is shown in surface-fixed coordinates. The surface-fixed coordinate is not frozen in inertial space but is rotating synchronized with the surface motion. In the end, the alignment angle is sufficiently controlled to zero and the touchdown sequence successfully demonstrated. The required ΔV is estimated around 0.34 m/s in this example (bottom of Fig. 7) with the lateral initial position error assumed to be 100 m. The correction interval is every 60 s with the filter time constant of

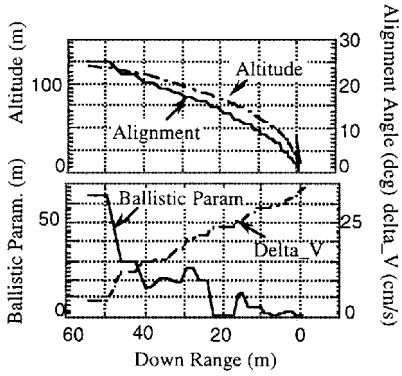

Fig. 7 Phase TD: guidance results.

50 s. During phase D-II prior to DDP the descent velocity is reduced to 10 cm/s. A summary of 100 cases with the random LOS rate noise is presented in Table 5.

In Table 5, no asteroid gravity field is assumed except cases 6–11. Because the descent velocity is slow (10 cm/s), the spacecraft stays close to the surface for almost half an hour. Consequently, an accompanying gravity loss will be added to the correction ΔV. The gravity compensation here is the feedforward scheme developed earlier in the text. The basic guidance properties remain unchanged, while the ΔV cost is raised to 6.6 m/s. Some stability dependency on the filter time constant, as well as the descent velocity, is observed in case 2. Both degrade the guidance performance, causing wider dispersions. As case 4 indicates, the guidance performance is found to be robust for the initial position error. The scheme is still valid even in the case when the correction interval is doubled. Case 7 deals with the higher potential field, in which C_{20} and C_{22} are calculated to be -0.01 and -0.03, respectively, for the target body. The irregularity alleviates the correction ΔV slightly with the degraded guidance properties. As cases 8 and 9 indicate, the scheme developed is found still insensitive to the spin state of the target body. Even in the case where the mass of the target body is 1.2 times as much as postulated, the guidance scheme still functions successfully as case 10 shows. Case 11 also demonstrates that the guidance performance is insensitive to the execution error of 5%. Because the last maneuver may occur at the altitude of 6 m above the surface, the final dispersion of approximately 2 m inevitably takes place. These robust features derive from the closed-loop guidance properties. In addition to the straightforward gravity compensation already developed, the following integration feedback loop is introduced to cope with the potential field effect:

$$\Delta V_{\text{comp},k+1} = \Delta V_{\text{comp},k} + k_1(\rho_k \dot{\boldsymbol{e}}) + k_2\left(v^* - \frac{\rho_k - \rho_{k-1}}{\Delta T_c}\right) \quad (21)$$

The entire simulation program was developed to ensure the sequence starting from the home position located at the distance of 50 km to the surface. This total simulation incorporates the asteroid gravity field, as well as the potential harmonics of C_{20} and C_{22}. A Monte Carlo-like survey of 20 cases was conducted. The total ΔV averaged is 12.26 m/s, which is a little higher than the sum of those associated with phases D-I and TD simulations in Tables 4 and 5. This is because the phase D-I simulations presented before did not take the gravity loss into account. The mathematical upper limit of ΔV from infinity to the distance r_f is assessed by $\mu/(v \cdot r_f)$, and it is 13.3 m/s when v is 10 cm/s. Inasmuch as the actual path is not a constant-velocity path, the total ΔV amount is lowered in this case. The resulting mean alignment angle is 5.15 deg with the final dispersion of 62.9 cm, which are smaller than those in Table 5 because the touchdown point is different; however, these errors are within the range of dispersions given in case 7 of Table 5. Each of these cases demonstrates that the strategies developed in the paper function as expected.

Conclusions

The preliminary analysis on combined autonomous navigation and guidance strategies around an asteroid are presented. Six innovations were discussed: 1) an aligned intercept guidance, 2) a combined range estimation along with corrections without a range sensor, 3) a strategic building of the flight phases, 4) an image processing of LOS shift information instead of tracking characteristic points, 5) stability and accuracy analysis associated with the strategies developed here, and 6) the correction interval, spacing analysis. What is important is that not all of the orbital information is required for the guidance to a small body. The navigation strategy was re-examined from the guidance aspects. The strategy developed is sufficiently concise and efficient that even the smallest spacecraft such as the MUSES-C can be equipped with such a scheme. Some comprehensive numerical illustrations, taking gravity into account, were given to support the discussion.

References

[1]Kawaguchi, J., Uesugi, K., Fujiwara, A., Kuninaka, H., and Hashimoto, T., "Sample and Return Mission in 2002 to Nereus via Electric Propulsion," 46th International Astronautical Congress, International Astronautical Federation, Paper IAF-95-Q.5.05, Oslo, Norway, Oct. 1995.

[2]Richter, L. O., Hohe, L., and Krupp, T., "Small Landing Vehicles for Minor Solar System Bodies," Second IAA International Conf. on Low-Cost Planetary Missions, International Academy of Astronautics, Preprint, IAA-L-0513, Applied Physics Lab., Johns Hopkins Univ., April 1996.

[3]Scheeres, D. J., "Satellite Dynamics About Asteroids," *Advances in the Astronautical Sciences*, Vol. 87, No. 1, 1994, pp. 275–292; also AAS-94-112.

[4]Broucke, R. A., and Scheeres, D. J., "Computing Orbits Around an Ellipsoid of Revolution," *Advances in the Astronautical Sciences*, Vol. 87, No. 1, 1994, pp. 423–440; also AAS-94-161.

[5]Guillaud, V., and de Lafontaine, J., "Navigation in the Vicinity of a Cometary Nucleus," *Advances in the Astronautical Sciences*, Vol. 69, 1989, pp. 743–761; also American Astronomical Society/Goddard Space Flight Center, International Symposium on Orbital Mechanics and Mission Design, AAS-89-207-1, Goddard Space Flight Center, Greenbelt, MD, April 1989.

[6]de Lafontaine, J., "Autonomous Spacecraft Navigation and Control for Comet Landing," *Journal of Guidance, Control, and Dynamics*, Vol. 15, No. 3, 1992, pp. 567–576.

[7]Riedel, J. E., Bhaskaran, S. E., Synnott, S. P., Bollman, W. E., and Null, G. W., "An Autonomous Optical Navigation and Control System for Interplanetary Exploration Missions," Second IAA International Conf. on Low-Cost Planetary Missions, International Academy of Astronautics, Preprint, IAA-L-0506, Applied Physics Lab., Johns Hopkins Univ., April 1996.

[8]Scheeres, D. J., "Close Proximity and Landing Operations at Small Bodies," *AIAA/AAS Astrodynamics Specialists Conference* (San Diego, CA), 1996, pp. 99–109 (AIAA Paper 96-3580).

[9]Zheng, Q., and Chellappa, R., "A Computational Vision Approach to Image Registration," *IEEE Transactions on Image Processing*, Vol. 2, No. 3, 1993, pp. 311–326.

[10]Bhaskaran, S., Riedel, J. E., and Synnott, P., "Demonstrations of Autonomous Orbit Determination Around Small Bodies," AAS/AIAA Astrodynamics Conf., Paper AAS 95-387, Halifax, NS, Canada, Aug. 1995.

[11]Misu, T., Hashimoto, T., and Ninomiya, K., "Autonomous Guidance of Spacecraft Based on Visual Feedback and Laser Ranging," Second International Conf. on Low-Cost Planetary Missions, International Academy of Astronautics, Preprint, IAA-0507, Applied Physics Lab., Johns Hopkins Univ., April 1996.

[12]Miller, J. K., Williams, B. G., Bollman, W. E., Davis, R. P., Helfrich, C. E., Scheeres, D. J., Synnott, S. P., Wang, T. C., and Yeomans, D. K., "Navigation Analysis for Eros Rendezvous and Orbital Phases," *Journal of the Astronautical Sciences*, Vol. 43, No. 4, 1995, pp. 453–476.

[13]Scheeres, D. J., Williams, B. G., Bollman, W. E., Davis, R. P., Helfrich, C. E., Synnott, S. P., and Yeomans, D. K., "Navigation for Low-Cost Missions to Small Solar-System Bodies," *Acta Astronautica*, Vol. 35, Suppl., 1995, pp. 211–220.

[14]Miller, J. K., Weeks, C. J., and Wood, L. J., "Orbit Determination of the Comet Rendezvous/Asteroid Flyby Mission: Post Rendezvous Phases," AIAA Paper 89-0348, Jan. 1989.

[15]Noton, M., "Orbital Strategies Around a Comet by Means of a Genetic Algorithm," *Journal of Guidance, Control, and Dynamics*, Vol. 18, No. 5, 1995, pp. 1217–1220.

[16]Kawaguchi, J., "An Optical Terminal Guidance and Navigation Strategy in the Asteroid Rendezvous Mission," *AIAA/AAS Astrodynamics Specialists Conference* (San Diego, CA), 1996, pp. 70–76 (AIAA Paper 96-3577).

[17]Kawaguchi, J., Hashimoto, T., Misu, T., and Sawai, S., "An Autonomous Optical Guidance and Navigation Around the Asteroid," 47th International Astronautical Congress, International Astronautical Federation, Paper IAF-96-A.4.03, Beijing, PRC, Oct. 1996.

[18]Kawaguchi, J., and Matsuo, H., "Low-Thrust Flyby Guidance and an Extended Optimal Spacing Rule," *Journal of Guidance, Control, and Dynamics*, Vol. 19, No. 2, 1996, pp. 347–354.